



Published in final edited form as:

Acta Neuropathol. 2018 October ; 136(4): 607–620. doi:10.1007/s00401-018-1873-4.

Alpha-Synuclein Delays Mitophagy and Targeting Miro Rescues Neuron Loss in Parkinson's Models

Atossa Shaltouki^{#1}, Chung-Han Hsieh^{#1}, Min Joo Kim¹, and Xinnan Wang^{1,*}

¹Department of Neurosurgery, Stanford University School of Medicine, Stanford, CA.

[#] These authors contributed equally to this work.

Abstract

Alpha-synuclein is a component of Lewy bodies, the pathological hallmark of Parkinson's disease (PD), and is also mutated in familial PD. Here, by extensively analyzing PD patient brains and neurons, and fly models, we show that alpha-synuclein accumulation results in upregulation of Miro protein levels. Miro is a motor/adaptor on the outer mitochondrial membrane that mediates mitochondrial motility, and is removed from damaged mitochondria to facilitate mitochondrial clearance via mitophagy. PD patient neurons abnormally accumulate Miro on the mitochondrial surface leading to delayed mitophagy. Partial reduction of Miro rescues mitophagy phenotypes and neurodegeneration in human neurons and flies. Upregulation of Miro by alpha-synuclein requires an interaction via the N-terminus of alpha-synuclein. Our results highlight the importance of mitochondria-associated alpha-synuclein in human disease, and present Miro as a novel therapeutic target.

Keywords

Parkinson; alpha-synuclein; Miro; mitochondria; mitophagy; iPSC; fly; dopaminergic

Introduction

Parkinson's disease (PD) is the second most common neurodegenerative disease, and is characterized by selective loss of dopaminergic neurons in the substantia nigra. Although the underlying pathogenesis still remains elusive, several PD-causing genes have been shown to control damaged mitochondrial clearance via mitophagy [19, 24, 25, 42]. These genes include *PINK1*, *Parkin*, and *LRRK2*. Because mitochondrial health and quality control are central to neuronal homeostasis, function, and survival [19, 25, 39], it is enticing to hypothesize that impairments in clearing damaged mitochondria may contribute to PD broadly, and not just in those specific genetic forms.

*Correspondence: xinnanw@stanford.edu, 6507249282 (t), 6507257813(f).

AUTHOR CONTRIBUTIONS

A.S., C.H., and M.K. designed and performed experiments, and made figures. X.W. conceived and supervised the project, designed the experiments, and wrote the paper with the assistance from all authors.

NO COMPETING FINANCIAL INTERESTS

PD patients bearing mutations in *PINK1*, *Parkin*, and *LRRK2* account for a small fraction of total cases [13]. Notably, nearly all cases of PD contain Lewy bodies in the brain. The major constituent of Lewy bodies is alpha-synuclein (α -syn) protein [21]. Mutations or amplifications of *alpha-synuclein* (*SNCA*) gene are also a cause of familial PD [31]. Physiologically, α -syn is largely a cytosolic protein enriched in neuronal synapses, and acts to maintain synaptic transmission [1, 3, 6]. α -Syn levels increase in dopaminergic neurons with factors such as age and PD [4, 10, 12]. Elevated levels of α -syn may disrupt multiple intracellular transport pathways [1]. Emerging studies suggest that a fraction of α -syn can localize to the mitochondria and influence mitochondrial functions, and that *SNCA* genetically interacts with *PINK1/Parkin* [9, 12, 16, 18, 20, 23, 27, 28, 30]. The precise cellular consequences of α -syn's association with mitochondria and its role in the pathogenesis, especially in the context of PD patients, are under-characterized.

Mitochondrial motility is tightly controlled by the cell to meet energy demands and reduce oxidative stress. Miro is a motor/adaptor on the outer mitochondrial membrane (OMM) that anchors mitochondria to microtubule motors [17, 34]. In order to move along microtubules, healthy mitochondria require a certain amount of Miro on the OMM. In contrast, depolarized, damaged mitochondria need to remove Miro quickly from the OMM to stop mitochondrial motility and initiate mitophagy [19, 42]. Subsequently, Miro becomes degraded by the proteasome. We and others have shown that the PD-causing genes *LRRK2*, *PINK1*, and *Parkin* target Miro for removal from the OMM of damaged mitochondria [19, 22, 42]. This suggests that Miro may be broadly affected in PD. However, whether α -syn is linked to Miro remains obscure. Here, we provide direct evidence that α -syn accumulation leads to an increase in Miro on the OMM and delays mitophagy.

Materials and Methods

Fly stocks

The following fly stocks were used: *Actin-GAL4*, *elav-GAL4*, *TH-GAL4*, *UAS-SNCA*, *UAS-SNCA-A53T* [37], *UAS-DMiro-RNAi* (VDRC 106683).

Fly Behavior Assay

Methods are similar as described in [38]. Briefly, climbing ability was quantified by time it took adult flies to climb 8 centimeters. Flying ability was defined as the ability of the adult fly to fly: If the fly was able to fly it was scored as a 1; otherwise it was scored as a 0.

Human Postmortem Brain Analysis

The ethical guidelines for human materials by Stanford University were followed throughout the study. Frozen sections from the frontal and temporal cortices were obtained from the Banner Sun Health Research Institute with patient history and pathological findings. Control brains were from subjects who died of non-neurological causes and displayed no signs of brain pathology. Brain samples were shipped on dry ice and stored at -80°C until they were sonicated in ice-cold PBS supplemented with EDTA-free protease inhibitor cocktail (05892791001; Roche). Brain tissues were then homogenized in Triton X-100 lysis buffer (50 mM Tris, 150 mM NaCl, 1 mM DTT, and 1% Triton X-100) with 0.25 mM

phenylmethanesulfonylfluoride (PMSF, P7626; Sigma-Aldrich) and protease inhibitor cocktail. After centrifugation at 17,000 g for 10 min, the detergent-soluble supernatant was run in SDS-PAGE (see Supplementary Methods). Note that the detergent-insoluble pellet should contain Lewy bodies [33]. For immunostaining of the substantia nigra, paraffin-embedded slides were obtained from the Banner Sun Health Research Institute, and deparaffinized by being immersed with 2 changes of xylene for 5 min, followed by rehydration with a sequential dilution of ethanol (100%, 95%, 70%, 50%, 0%) for 3 min, repeated twice at each concentration. Then slides were rinsed with 1×PBS for 10 min, and immersed in sodium citrate buffer (10 mM sodium citrate, 0.05% Tween 20, pH 6.0) at 95°C for 20 min for epitope retrieval. Slides were next rinsed with 1×PBS for 10 min, and blocked in PBS with 0.3% Triton X-100 and 5% normal donkey serum for 60 min. Slides were immunostained with anti-TH (NB300–110; Novus Biologicals) at 1:400, anti-Miro1 (HPA010687; Sigma-Aldrich) 1:500, anti-ATP5 β (Ab14730; Abcam) at 1:500, anti-MCAD (Ab110296, Abcam) at 1:250, or mouse anti- α -syn (211, sc-12767; Santa Cruz) at 1:400 [11], and Alexa fluorophore-conjugated IgG (Jackson ImmunoResearch) at 1:1000. Samples were imaged at room temperature with a 63×/N.A.1.30 oil Plan-Apochromat objective on a Leica SPE laser scanning confocal microscope (Leica Microsystems), with identical imaging parameters among different subjects in a blind fashion. Images were processed with ImageJ (Ver. 1.48, NIH) using only linear adjustments of contrast and color.

Constructs

The following constructs were used: mito-dsRed [19]; EGFP [41]; pA1T7-DMiro [41], pA1T7-DMiroTM [17], mito-mkeima [5], Myc-Miro1 [14], EGFP-SNCA (WT and A53T, Addgene No.: 40822 and 40823) [15], and HA-SNCA (WT and A53T, Addgene No.: 40824 and 40825). SNCA truncation constructs were made by PCR amplification of N-terminal fragment (1–95) and C-terminal fragment (42–140) of human *SNCA*. The amplified fragments were gel purified and subcloned into the HindIII and EcoRI site of pHM6, and the resulting constructs were sequenced.

Quantitative Real-Time PCR (qPCR) and Reverse Transcription PCR (RT-PCR)

RNA was extracted using Qiagen RNeasy Plus Mini Kit according to manufacturer's instructions. For qPCR, reactions were carried out on the StepOnePlusTM instrument (Thermo Fisher Scientific, CA) using iTaqTM Universal SYBR[®] Green supermix (Bio-Rad, CA) according to manufacturer's instructions. Reactions were conducted in triplicate for each sample. Human *GAPDH* and β -*actin* were amplified as internal standards. Reported values were calculated using Δ Ct method and normalized against endogenous *GAPDH*. The following primers were used:

Nanog 50 forward: 5'-TGAACCTCAGCTACAAACAG-3'

Nanog 50 reverse: 5'-TGGTGGTAGGAAGAGTAAAG-3'

OCT 4 END forward: 5'-CCTCACTTCACTGCACTGTA-3'

OCT 4 END reverse: 5'-CAGGTTTTCTTTCCCTAGCT-3'

OCT 4 TOTAL forward: 5'-AGCGAACCAGTATCGAGAAC-3'

OCT 4 TOTAL reverse: 5'-TTACAGAACCACACTCGGAC-3'

SOX2 END forward: 5'-CCCAGCAGACTTCACATGT-3'

SOX2 END reverse: 5'--CCTCCCATTTCCTCGTTTT-3'

SOX2 TOTAL forward: 5'-AGCTACAGCATGATGCAGGA-3'

SOX2 TOTAL reverse: 5'--GGTCATGGAGTTGTACTGCA-3'

SNCA forward: 5'- AGCGGACCTCCACAAGTAACGAAT-3'

SNCA reverse: 5'-TTGGCATCTGTCTTCCTCCCAAGT-3'

GAPDH forward: 5'- ACCACAGTCCATGCCATCAC-3'

GAPDH reverse: 5'- TCCACCACCCTGTTGCTGT-3'

Miro1 forward: 5'- GGGAGGAACCTCTTCTGGA-3'

Miro1 reverse: 5'- ATGAAGAAAGACGTGCGGAT-3'

β -Actin forward: 5'- TGAAGTGTGACGTGGACATC-3'

β -Actin reverse: 5'- GGAGGAGCAATGATCTTGAT-3'

SeV+ forward: 5'- GGATCACTAGGTGATATC GAGC-3'

SeV+ reverse: 5'- ACCAGACAAGAGTTTAAGAGATATGTATC-3'

Live Image Acquisition and Quantification

As described previously [40–42], neurons on glass coverslips were placed in a 35-mm petridish containing the Hibernate E low-fluorescence medium (BrainBits) on a heated stage of 37°C, and imaged with a 63 \times /N.A.0.9 water-immersion objective with excitation at 561 nm or 488 nm. Time-lapse movies were obtained continually with 3–5 sec intervals before and after Antimycin A (100 μ M, Sigma-Aldrich) was added. Axons longer than 50 μ m were selected for recording. Movie length ranged from 120 to 300 min. TMRM (T668, Molecular Probes) was applied at 250 nM for 10 min when needed. For quantification, kymographs were generated from time-lapse movies by ImageJ, representing a 100-sec period either right before or following different time points after addition of Antimycin A. Each kymograph was then imported into a macro written in Labview (NI, TX), and individual mito-dsRed puncta were traced using a mouse-driven cursor at the center of the mito-dsRed object. Using Matlab (The MathWorks, MA), we determined the following parameters: 1) the instantaneous velocity of each mitochondrion, 2) the average velocity of those mitochondria that are in motion, 3) the percent of time each mitochondrion is in motion, 4) stop frequency, and 5) turn back frequency. The intensity of mitochondria is measured using ImageJ.

Mitochondrial Isolation

Mitochondria were isolated from cultured HEK cells as described previously [19, 41]. Briefly, cells were mechanically homogenized with a Dounce homogenizer in 750 μ l isolation buffer (200 mM sucrose, 10 mM TRIS/MOPS, pH 7.4). After centrifugation at 500 g for 10 min, crude supernatant was spun at 10,000 g for 10 min to pellet intact mitochondria. Mitochondrial pellet was washed twice with isolation buffer. After this step,

supernatant was referred to “cytosolic fraction”, and pellet was resuspended in 50 μ l RIPA lysis buffer with 0.25 mM PMSF and protease inhibitors referred to “mitochondrial fraction”.

Immunocytochemistry and Confocal Microscopy

Cells were fixed in 2–4% paraformaldehyde (Electron Microscopy Sciences, Hatfield, PA), or 90% methanol for 15 min, then washed three times in PBS, and blocked in PBS with 0.1% Saponin (Sigma-Aldrich) or 0.1% Triton X-100, 4% Bovine Serum Albumin, and 5–10% normal goat serum for 60 min. Cells were then immunostained with anti-TH (MAB318; EMD Millipore, and P40101; Pel-Freez) at 1:250–500, anti-TUJ-1 (T8660 and T2200; Sigma) at 1:1,000, anti-Nanog (14–5768-82; eBioscience) at 1:100, anti-SOX2 (MAB4343; EMD Millipore) at 1:1,000, anti-SMA (A2547; Sigma) at 1:500, anti-AFP (A8452; Sigma) at 1:500, anti-Tra160 (14–8863-82; eBioscience) at 1:60, anti-OCT4 (ab19857; Abcam) at 1:1,250, anti- α -syn (211, sc-12767; Santa Cruz) at 1:500 [11], anti-FOXA2 (sc-6554; Santa Cruz) at 1:1,000, anti-LMX1A (Ab139726; Abcam) at 1:250, or anti-Miro1 (HPA010687; Sigma-Aldrich) at 1:500, and Alexa fluorophore-conjugated IgG (Jackson ImmunoResearch Laboratories or Life technologies) at 1:500–1,000. Nuclei were visualized by staining with Hoechst (H3570; Life Technologies) at 1:10,000. Adult fly brains were dissected in PBT (0.3% Triton X-100 in PBS), and incubated with fixative solution (4% formaldehyde in PBT) for 20 min. Fixed samples were immunostained with mouse anti-TH (MAB318; EMD Millipore) at 1:200. Samples were imaged at room temperature with a 20 \times /N.A.0.60 or a 63 \times /N.A.1.30 oil Plan-Apochromat objective on a Leica SPE laser scanning confocal microscope (JH Technologies), with identical imaging parameters among different genotypes in a blind fashion. Images were processed with ImageJ (Ver. 1.48, NIH) using only linear adjustments of contrast and color.

Induced Pluripotent Stem Cells (iPSCs), Neuronal Differentiation, and Western Blotting in Supplementary Methods.

Statistical Analysis—Throughout the paper, the distribution of data points is expressed as box-whisker plots or dot-plots, except otherwise stated. The One-Way ANOVA Post-Hoc Tukey test was performed for comparisons among multiple groups. The Mann-Whitney *U* test was performed for comparisons between two groups. The Chi Square Test was performed for flying tests.

Results

Miro Protein Is Upregulated in PD Postmortem Brains Correlating with α -Syn Upregulation.

We tested the possibility that increased levels of α -syn in the aging PD brain perturbs Miro regulation. We immunoblotted Miro1 protein in lysates of the frontal and temporal cortices of postmortem brains from twenty PD patients aged 70–91 years, and twenty age-matched healthy controls (Supplementary Fig. 1a). Eighteen patients were apparently sporadic, and two patients have family history but with unknown genetic mutations (Supplementary Fig. 1a). We found that protein levels of both Miro1 and α -syn were significantly upregulated in PD patients as compared to controls, while other OMM markers including Mitofusin2 and VDAC, and kinesin heavy chain (KHC) which forms a complex with Miro, remained

unchanged (Fig. 1a-c, Supplementary Fig. 1b, 2a). Interestingly, we observed that the matrix protein, ATP synthase subunit β (ATP5 β), was upregulated in the temporal cortex (Fig. 1c, Supplementary Fig. 2a), which suggests a possibility of inefficient mitophagy in the aging PD brain. It appears that the OMM proteins Mitofusin2 and VDAC are otherwise unaffected, probably because Mitofusin2 and VDAC are digested through proteasomes rather than lysosomes during mitophagy [8] and their degradation still occurs in those PD cases. The protein level of Miro1 significantly correlated with that of α -syn, but not with gender, age, or postmortem delay (Fig. 1d-e, Supplementary Fig. 1c-e, 2b-d).

We next immunostained Miro1 in the substantia nigra from five PD patients and five matched healthy controls (Supplementary Fig. 1a). The specificity of the immunostaining signals of anti-Miro1 was verified in human neurons when *Miro1* was knocked down [19] (and described later). Miro1 and α -syn immunofluorescence was both significantly higher in TH-positive dopaminergic neurons in PD patients compared to controls (Fig. 2). The matrix proteins ATP5 β and medium-chain acyl-CoA dehydrogenase (MCAD) were also upregulated in PD patients (Fig. 2), which could be due to an impairment in mitochondrial clearance. Taken together, Miro1 and α -syn proteins accumulate in postmortem brains of idiopathic PD.

Miro Protein Is Upregulated in Human Neurons and Flies Expressing α -Syn.

We next proceeded to validate our findings from human brains in complementary cultured human cell and *in vivo* models. We found that in HEK293T cells overexpressing wild-type *SNCA* or pathogenic *SNCA-A53T*, endogenous Miro1 was significantly upregulated, while the mitochondrial markers Mitofusin2, Drp1, VDAC, and ATP5 β , and PD-linked proteins LRRK2, PINK1, and Parkin were unaltered (Fig. 3a). Misregulation of Miro1 occurred at the protein level, since *Miro1* mRNA levels were unaffected (Supplementary Fig. 2e). We also expressed human wild-type *SNCA* or pathogenic *SNCA-A53T* in flies [37] and detected endogenous *Drosophila* Miro (DMiro) levels [38]. Expression of α -syn, either ubiquitously by *Actin-GAL4* or selectively in neurons by *elav-GAL4*, resulted in an upregulation of DMiro protein in 15-day old adult flies (Fig. 3b). This upregulation was specific to DMiro, because additional mitochondrial markers including milton (the *Drosophila* ortholog of TRAK1/2), Marf (the *Drosophila* homolog of Mitofusin), OPA1, MIC60, and ATP5 β were not affected (Fig. 3b). Next, we examined Miro1 protein levels in iPSC-derived neurons from healthy human subjects and PD patients harboring *SNCA* mutations. Because those neurons converted from human patients express endogenous mutant α -syn protein, this system circumvents potential confounds caused by overexpression of α -syn. We used three iPSC lines reprogrammed from PD patients bearing *SNCA* mutations: *SNCA-A53T-I* (generated in house; Supplementary Fig. 3–4); *SNCA-A53T-II* (NINDS repository; ND50049); and *SNCA-triplication* (NINDS repository; ND34391). We also included three wild-type control iPSC lines: *Wild-type-I* [19]; *Wild-type-II* (NINDS repository; ND41864); and *Wild-type-III* (Stanford Stem Cell Core). We differentiated iPSCs to neurons expressing tyrosine hydroxylase (TH), the rate-limiting enzyme for dopamine synthesis (Supplementary Fig. 4a-d) as previously described [19], and imaged axons at day 22–26 after differentiation. We confirmed a significant increase in the number of cells immune-positive for endogenous α -syn protein in all three pathogenic

SNCA lines (Supplementary Fig. 4e). We then transiently transfected those neurons with mito-dsRed to label mitochondria and immunostained endogenous Miro1 [19]. In neuronal axons, Miro1 co-localized with mito-dsRed and its expression on mitochondria was significantly upregulated in all three pathogenic *SNCA* lines (Fig. 3c). We confirmed this upregulation of Miro1 protein in mutant neurons by immunoblotting (Fig. 3d). Elevation of Miro1 protein was not due to increased *Miro1* mRNA expression (Supplementary Fig. 5a). In summary, Miro is upregulated in flies and human neurons with genetic mutations in *SNCA*.

Partial Reduction of Miro Rescues Mitophagy Phenotypes and Neurodegeneration in iPSC-Derived Neurons with *SNCA* mutations.

We explored the cellular consequences of upregulation of Miro on both polarized and depolarized mitochondria. On polarized mitochondria, upregulation of Miro may increase mitochondrial motility. To test this possibility, we live-imaged mitochondrial movement labeled by mito-dsRed in neuronal axons. At the steady state, the mitochondrial membrane potential (Ψ_m), detected by TMRM staining, was higher in iPSC-derived *SNCA-A53T* neurons compared to wild-type neurons (Supplementary Fig. 5b; no treatment). We did not detect enhanced mitochondrial motility in *SNCA-A53T* neurons (Supplementary Fig. 5c-d; no treatment) despite higher Miro protein levels in those neurons (Fig. 3c), which is consistent with several observations in rodent neurons showing that mild overexpression of Miro does not increase mitochondrial motility [41, 42].

On depolarized mitochondria, accumulation of Miro could delay the arrest of mitochondria and the initiation of mitophagy (Fig. 4a), because Miro needs to be removed in a timely fashion for mitophagy to start [19]. To test this hypothesis, we applied the Complex III inhibitor Antimycin A to trigger mitophagy [2, 19, 42] in iPSC-derived neurons. We confirmed that application of Antimycin A for 15 minutes significantly depolarized the Ψ_m (Supplementary Fig. 5b). Following Antimycin A treatment, whereas in wild-type neurons mitochondrial motility significantly stopped in both anterograde and retrograde directions at 25 minutes, in *SNCA-A53T* neurons mitochondria did not stop movement until 70 minutes (Supplementary Fig. 5c-d). The mitochondrial intensity in wild-type neurons was efficiently reduced at 70 minutes after treatment, while at the same time in *SNCA-A53T* neurons mitochondria were not significantly degraded (Supplementary Fig. 5c, e). This delay in arresting and clearing damaged mitochondria in *SNCA-A53T* neurons has also been observed by us in iPSC-derived neurons from PD patients with the *LRRK2G2019S* mutation [19], and occurred in isogenic iPSC-derived human neurons knocking out *Parkin* (Supplementary Fig. 5f-h). Importantly, LRRK2 and Parkin have been both previously shown to target Miro and mediate mitophagy [19, 42]. These live-imaging results suggest that mitophagy is also delayed in *SNCA-A53T* neurons.

If this mitochondrial phenotype is due to upregulation of Miro (Fig. 3c), one simple approach to rescue the phenotype might be to mildly lower basal Miro levels by RNAi [19]. To test this hypothesis, we transfected neurons with mito-dsRed, EGFP, and RNA duplexes at day 20–22 after neuronal induction, and 3 days later we imaged the neurons. Neurons positive for both mito-dsRed and EGFP have also likely obtained RNA duplexes

[19, 41, 42]. The specificity of Miro1 siRNA in human iPSC-derived neurons has been validated by our previous studies [19]. We used non-targeting siRNA as a negative control. We directly measured Miro1 removal rates from depolarized mitochondria by immunostaining endogenous Miro1 at different time points following Antimycin A treatment. We consistently found that with control RNAi the basal levels of Miro1 were higher in *SNCA-A53T* neurons than in wild-type (Fig. 3c, 4b). Notably, after depolarization it took much longer for *SNCA-A53T* neurons to remove Miro1 than for wild-type, both because there was more Miro1 to start with and the Miro1 removal rate was slower within the first 25 minutes (Fig. 4b). This delay in removing Miro from damaged mitochondria is consistent with our live-imaging findings that damaged mitochondria arrest and clearance are delayed in *SNCA-A53T* neurons (Supplementary Fig. 5c-e).

Miro1 RNAi reduced the Miro1 level to $66.76 \pm 4.625\%$ and $65.40 \pm 6.220\%$ in wild-type and *SNCA-A53T* neurons, respectively (Fig. 4b). Importantly, Miro1 RNAi significantly shortened the time to remove Miro1 in *SNCA-A53T* neurons (Fig. 4b). We next live monitored mitophagy in those neurons using a ratiometric pH sensitive biosensor mito-mkima [5, 19]. Fusion of mitochondria-containing autophagosomes with acidic lysosomes increases the fluorescent ratio of mito-mkima excited by 561 nm over 488 nm. While it took wild-type neurons 65 minutes to increase the ratio, it took *SNCA-A53T* neurons 150 minutes; reduced to 90 minutes by Miro1 RNAi (Fig. 4c). These results provide evidence that lowering basal Miro1 levels promotes Miro1 removal and mitophagy in *SNCA-A53T* neurons.

We now have a way to more efficiently initiate mitophagy and clear damaged mitochondria in *SNCA-A53T* neurons by partial reduction of Miro1 (Fig. 4c). We next explored whether this approach protects those neurons from stress. We transfected neuronal cultures with EGFP, and applied Antimycin A for 6 hours to induce stress [19]. We identified EGFP-positive neurons by morphology [19, 42] and dopaminergic neurons by TH-immunostaining (Fig. 4d). Consistent with iPSC-derived neurons bearing other PD mutations [7, 19, 26], *SNCA-A53T* neurons were more sensitive to stress than wild-type (Fig. 4d). Notably, TH-positive *SNCA-A53T* neurons exhibited even more vulnerability than TH-negative *SNCA-A53T* neurons ($5.12 \pm 1.577\%$ of TH-positive and $31.33 \pm 2.291\%$ of TH-negative neurons were alive after treatment, $P < 0.0001$, Fig. 4d). Miro1 RNAi completely rescued stress-induced degeneration of those neurons (Fig. 4d). Taken together, pathogenic *SNCA-A53T* delays Miro1 removal from damaged mitochondria, impairing the induction of mitophagy, and increases susceptibility to stress in human neurons; lowering Miro1 levels rescues these defects.

Partial Reduction of Miro Rescues Locomotion Deficits and Dopaminergic Neurodegeneration in Flies Expressing Human *SNCA*.

We also tested the neuroprotective effect of lowering Miro protein levels *in vivo*. Transgenic *Drosophila* overexpressing human α -syn exhibit dopaminergic neurodegeneration [37]. Thus, we used the fruit fly as an *in vivo* model of α -syn-induced neurodegeneration. We knocked down DMiro by RNAi in flies [19] (Supplementary Fig. 6a) overexpressing wild-type *SNCA* or *SNCA-A53T* in dopaminergic neurons driven by TH-GAL4. Adult flies

expressing *SNCA-A53T*, but not wild-type *SNCA*, displayed defective climbing ability as early as 5 days after eclosion (Fig. 5a). Adult flies expressing either wild-type *SNCA* or *SNCA-A53T* showed impaired flying ability (Fig. 5b). In the adult brain, age-dependent dopaminergic neurodegeneration was detected in the clusters of paired posterior lateral 1 (PPL1) when either wild-type *SNCA* or *SNCA-A53T* was expressed, and in the clusters of paired posterior medial 1/2 (PPM1/2) when *SNCA-A53T* but not wild-type was expressed (Fig. 5c, Supplementary Fig. 6b). Because both wild-type *SNCA* and *SNCA-A53T* cause DMiro upregulation in neurons, but the phenotype appears more severe with *SNCA-A53T* (Fig. 3b), these results suggest that the flying ability and dopaminergic neuronal survival in the PPL1 clusters may be more sensitive to upregulation of DMiro. Remarkably, all of the impaired climbing and flying abilities and dopaminergic neurodegeneration were fully rescued by DMiro RNAi (Fig. 5, Supplementary Movies 1–3). Therefore, partial inhibition of DMiro protects the locomotion, flying ability, and dopaminergic neuronal survival in an *in vivo* PD model.

The N-terminus of α -Syn Is Required to Interact with and Upregulate Miro.

We explored the molecular mechanisms underlying α -syn-dependent upregulation of Miro. Because we have shown that α -syn accumulation does not affect *Miro* mRNA expression (Supplementary Fig. 2e, 5a), α -syn should influence Miro at the protein level. Previous studies have provided evidence that α -syn can localize to the OMM [12, 18, 20, 23, 30], and thus α -syn may associate with Miro in the same complex to affect Miro turn-over. In HEK293T cells, we also detected exogenously-expressed wild-type α -syn and α -syn-A53T in both the mitochondrial and cytosolic fractions (Fig. 6a). By co-immunoprecipitations, we identified that Myc-Miro1 co-complexed with both wild-type HA- α -syn and HA- α -syn-A53T, but showed stronger binding to the latter (Fig. 6b). To map the domain of α -syn required for Miro interaction, we expressed HA-tagged full-length (FL) α -syn, amino acids 42–140, or amino acids 1–95 [6], in HEK293T cells along with Myc-Miro1. We found that α -syn (42–140) significantly disrupted the binding to Miro1 (Fig. 6c), suggesting that the N-terminus of α -syn is required for interaction with Miro1. We next expressed T7-tagged FL DMiro and DMiroTM (transmembrane domain deleted) along with HA- α -syn in HEK293T cells and determined their associations. DMiro has highly conserved domains and DMiroTM releases DMiro from the OMM to the cytosol [17]. We found that DMiroTM significantly reduced the binding to α -syn (Fig. 6d). Taken together, α -syn and Miro form a complex on the OMM.

We consistently observed upregulation of exogenously-expressed Myc-Miro1 by overexpression of HA- α -syn in HEK cells (Fig. 6b-c, Input). Deletion of the N-terminal amino acids 1–41 of α -syn compromised the ability of α -syn to upregulate Miro1 (Fig. 6c, Input). Therefore, the N-terminus of α -syn is essential both for binding to and for elevating Miro1 protein.

α -Syn's Impact on Miro Is Independent of the LRRK2 and PINK1-Parkin Pathways.

It is known that the PINK1-Parkin and LRRK2 pathways mediate Miro removal from the damaged mitochondrial surface to release Miro to the cytosol. Mitochondrial depolarization triggers interactions of Miro with LRRK2, PINK1, and Parkin, and these interactions

facilitate Miro removal (Fig. 6e) [19, 42]. It is possible that α -syn interferes with LRRK2 and the PINK1-Parkin axis to stabilize Miro on the OMM. Because PINK1 functions upstream of Parkin recruitment to Miro and damaged mitochondria [19], we determined whether α -syn disrupts Miro binding to Parkin or LRRK2. We expressed EGFP- α -syn and Myc-Miro1 in HEK cells, and applied CCCP, which depolarizes mitochondria, for 10 min [19, 42]. We discovered that the presence of excessive α -syn did not affect Myc-Miro1 interactions with either endogenous LRRK2 or Parkin following CCCP treatment (Supplementary Fig. 6c). Thus, α -syn does not significantly interrupt LRRK2 and Parkin recruitments to Miro on damaged mitochondria (Fig. 6e). This result suggests that the LRRK2 and PINK1-Parkin pathways are not influenced by α -syn accumulation, and is consistent with our observations in various α -syn-dependent PD models showing normal turn-over rates of Mitofusin/marf (Fig. 1, 3), a known target of PINK1/Parkin for proteasome degradation [8, 32].

Discussion

In this study, we have discovered that accumulation of α -syn results in an upregulation of Miro protein, in both postmortem brains and iPSC-derived neurons from PD patients, as well as in fly PD models. This work provides the first link of a central player in PD pathology to a crucial regulator of mitochondrial motility and quality control. This link reveals a new, unexplored layer of complexity that α -syn toxicity has in the aging brain via mitochondria-associated α -syn.

Upregulation of Miro delays mitochondrial clearance via mitophagy (Fig. 4, 6e). We have shown accumulation of Miro, and probably mitochondria in the substantia nigra and temporal cortex of human PD postmortem brains expressing elevated, endogenous α -syn (Fig. 1–2). Importantly, we did not find mitochondrial accumulation in HEK cells with transient expression of α -syn, young flies expressing α -syn, or in the frontal cortex of PD postmortem brains, although Miro upregulation is consistently observed in all of those models. A long-term insult from α -syn protein may be needed for damaged mitochondrial accumulation. It is also possible that different cells contain different amounts of damaged mitochondria. Cells that contain less damaged mitochondria may be more tolerant of impaired mitophagy. In contrast, dopaminergic neurons in the substantia nigra are constantly under energy crisis and various stresses owing to their unique axonal morphology, bioenergetics, and neuronal activities, and consequently their mitochondria may more often become damaged [29, 35, 36]. It is plausible that in those neurons even subtle disturbances in removing Miro and initiating mitophagy may accumulate defective mitochondria, and over time lead to neuronal cell death (Fig. 6e). We have shown that in iPSC-derived neurons Miro upregulation renders TH-positive neurons higher sensitivity to stress than TH-negative neurons (Fig. 4d). These results provide evidence that mitochondria in dopaminergic neurons experience more stress and thus those neurons may be more susceptible to accumulated Miro and resultant delayed mitophagy.

Remarkably, partial reduction of Miro by RNAi rescues locomotion defects and neurodegeneration in both flies and human neurons harboring pathogenic *SNCA* mutations. We and others have shown that Miro RNAi also alleviates neurodegeneration in human

neuron and fly PD models linked to pathogenic *LRRK2* and *PINK1* [19, 22]. Our results connecting Miro to α -syn and sporadic PD suggest that targeting Miro in PD could have broad and effective applications. Additionally, the novel phenotypic readouts that we have discovered can be used to screen for genes and pathways, chemicals, small molecules, and even diets which target Miro and mitophagy. It is important to note that a complete depletion of Miro would affect motility of polarized mitochondria, and thus a partial reduction while keeping the minimum amount of Miro on mitochondria required for movement should be the goal for future drug screens and for developing and optimizing Miro inhibitors.

We have shown that α -syn protein is incorporated into the membrane-associated Miro complex via the N-terminus of α -syn. Deletion of the first 41 amino acids does not completely abolish α -syn interaction with Miro1 in a heterologous system (Fig. 6c), suggesting that α -syn oligomerization or additional domains of α -syn may be involved. Because α -syn accumulation does not affect *Miro* mRNA expression (Supplementary Fig. 2, 5), α -syn could either facilitate embedding of newly-synthesized Miro protein into the OMM or prevent extraction of Miro from the OMM for cytosolic degradation [42]. These possibilities warrant future investigation. Our study demonstrates the importance of mitochondria-associated α -syn for PD, and positions mitochondria at the center of PD pathogenesis with Miro as a potentially straightforward therapeutic target.

Supplementary Material

Refer to Web version on PubMed Central for supplementary material.

ACKNOWLEDGEMENTS

We thank Drs. Renee Reijo Pera, Theo Palmer, Guangwen Wang (Stanford University Stem Cell Core, supported by California Institute for Regenerative Medicine, GC1R-06673-A to Dr. Michael Snyder), and the National Institute of Neurological Disorders and Stroke (NINDS) human and cell repository (<https://stemcells.ninds.genetics.org>) for iPSC lines, the Banner Sun Health Research Institute Brain and Body Donation Program of Sun City, Arizona for human postmortem brains, Dr. Leo Pallanck for flies, Dr. Alex Whitworth for antibodies, Dr. Thomas Südhof for constructs, and Ashley E. Gonzalez for technical support. This work was supported by the Michael J. Fox Foundation (X.W.), the Klingenstein Foundation (X.W.), the California Institute of Regenerative Medicine (X.W.), the National Institute of Health (X.W. RO1NS089583), and the Archer Fund (X.W.). The Brain and Body Donation Program is supported by the NINDS (U24 NS072026 National Brain and Tissue Resource for Parkinson's Disease and Related Disorders), the National Institute on Aging (P30 AG19610 Arizona Alzheimer's Disease Core Center), the Arizona Department of Health Services (211002, Arizona Alzheimer's Research Center), the Arizona Biomedical Research Commission (4001, 0011, 05-901 and 1001 to the Arizona Parkinson's Disease Consortium), and the Michael J. Fox Foundation.

REFERENCES

1. Abeliovich A, Gitler AD (2016) Defects in trafficking bridge Parkinson's disease pathology and genetics. *Nature* 539: 207–216 Doi 10.1038/nature20414 [PubMed: 27830778]
2. Ashrafi G, Schlehe JS, LaVoie MJ, Schwarz TL (2014) Mitophagy of damaged mitochondria occurs locally in distal neuronal axons and requires PINK1 and Parkin. *The Journal of cell biology* 206: 655–670 Doi 10.1083/jcb.201401070 [PubMed: 25154397]
3. Benskey MJ, Perez RG, Manfredsson FP (2016) The contribution of alpha synuclein to neuronal survival and function - Implications for Parkinson's disease. *Journal of neurochemistry* 137: 331–359 Doi 10.1111/jnc.13570 [PubMed: 26852372]
4. Betarbet R, Canet-Aviles RM, Sherer TB, Mastroberardino PG, McLendon C, Kim JH, Lund S, Na HM, Taylor G, Bence NF et al. (2006) Intersecting pathways to neurodegeneration in Parkinson's

disease: effects of the pesticide rotenone on DJ-1, alpha-synuclein, and the ubiquitin-proteasome system. *Neurobiology of disease* 22: 404–420 Doi 10.1016/j.nbd.2005.12.003 [PubMed: 16439141]

5. Bingol B, Tea JS, Phu L, Reichelt M, Bakalarski CE, Song Q, Foreman O, Kirkpatrick DS, Sheng M (2014) The mitochondrial deubiquitinase USP30 opposes parkin-mediated mitophagy. *Nature* 510: 370–375 Doi 10.1038/nature13418 [PubMed: 24896179]
6. Burre J, Sharma M, Sudhof TC (2012) Systematic mutagenesis of alpha-synuclein reveals distinct sequence requirements for physiological and pathological activities. *The Journal of neuroscience: the official journal of the Society for Neuroscience* 32: 15227–15242 Doi 10.1523/JNEUROSCI.3545-12.2012 [PubMed: 23100443]
7. Byers B, Cord B, Nguyen HN, Schule B, Fenno L, Lee PC, Deisseroth K, Langston JW, Pera RR, Palmer TD (2011) SNCA triplication Parkinson's patient's iPSC-derived DA neurons accumulate alpha-synuclein and are susceptible to oxidative stress. *PloS one* 6: e26159 Doi 10.1371/journal.pone.0026159 [PubMed: 22110584]
8. Chan NC, Salazar AM, Pham AH, Sweredoski MJ, Kolawa NJ, Graham RL, Hess S, Chan DC (2011) Broad activation of the ubiquitin-proteasome system by Parkin is critical for mitophagy. *Human molecular genetics* 20: 1726–1737 Doi 10.1093/hmg/ddr048 [PubMed: 21296869]
9. Chen L, Xie Z, Turkson S, Zhuang X (2015) A53T human alpha-synuclein overexpression in transgenic mice induces pervasive mitochondria macroautophagy defects preceding dopamine neuron degeneration. *The Journal of neuroscience: the official journal of the Society for Neuroscience* 35: 890–905 Doi 10.1523/JNEUROSCI.0089-14.2015 [PubMed: 25609609]
10. Chu Y, Kordower JH (2007) Age-associated increases of alpha-synuclein in monkeys and humans are associated with nigrostriatal dopamine depletion: Is this the target for Parkinson's disease? *Neurobiology of disease* 25: 134–149 Doi 10.1016/j.nbd.2006.08.021 [PubMed: 17055279]
11. Chung SY, Kishinevsky S, Mazzulli JR, Graziotto J, Mrejeru A, Mosharov EV, Puspita L, Valiulahi P, Sulzer D, Milner TA et al. (2016) Parkin and PINK1 Patient iPSC-Derived Midbrain Dopamine Neurons Exhibit Mitochondrial Dysfunction and alpha-Synuclein Accumulation. *Stem cell reports* 7: 664–677 Doi 10.1016/j.stemcr.2016.08.012 [PubMed: 27641647]
12. Di Maio R, Barrett PJ, Hoffman EK, Barrett CW, Zharikov A, Borah A, Hu X, McCoy J, Chu CT, Burton EA et al. (2016) alpha-Synuclein binds to TOM20 and inhibits mitochondrial protein import in Parkinson's disease. *Science translational medicine* 8: 342ra378 Doi 10.1126/scitranslmed.aaf3634
13. Erkkinen MG, Kim MO, Geschwind MD (2018) Clinical Neurology and Epidemiology of the Major Neurodegenerative Diseases. *Cold Spring Harbor perspectives in biology* 10: Doi 10.1101/cshperspect.a033118
14. Fransson S, Ruusala A, Aspenstrom P (2006) The atypical Rho GTPases Miro-1 and Miro-2 have essential roles in mitochondrial trafficking. *Biochemical and biophysical research communications* 344: 500–510 Doi 10.1016/j.bbrc.2006.03.163 [PubMed: 16630562]
15. Furlong RA, Narain Y, Rankin J, Wyttenbach A, Rubinsztein DC (2000) Alpha-synuclein overexpression promotes aggregation of mutant huntingtin. *The Biochemical journal* 346 Pt 3: 577–581 [PubMed: 10698681]
16. Gisbert S, Brehm N, Weil J, Seidel K, Rub U, Kern B, Walter M, Roeper J, Auburger G (2015) Potentiation of neurotoxicity in double-mutant mice with Pink1 ablation and A53T-SNCA overexpression. *Human molecular genetics* 24: 1061–1076 Doi 10.1093/hmg/ddu520 [PubMed: 25296918]
17. Glater EE, Megeath LJ, Stowers RS, Schwarz TL (2006) Axonal transport of mitochondria requires mltin to recruit kinesin heavy chain and is light chain independent. *The Journal of cell biology* 173: 545–557 Doi 10.1083/jcb.200601067 [PubMed: 16717129]
18. Guardia-Laguarta C, Area-Gomez E, Rub C, Liu Y, Magrane J, Becker D, Voos W, Schon EA, Przedborski S (2014) alpha-Synuclein is localized to mitochondria-associated ER membranes. *The Journal of neuroscience: the official journal of the Society for Neuroscience* 34: 249–259 Doi 10.1523/JNEUROSCI.2507-13.2014
19. Hsieh CH, Shaltouki A, Gonzalez AE, Bettencourt da Cruz A, Burbulla LF, St Lawrence E, Schule B, Krainc D, Palmer TD, Wang X (2016) Functional Impairment in Miro Degradation and Mitophagy Is a Shared Feature in Familial and Sporadic Parkinson's Disease. *Cell stem cell* 19: 709–724 Doi 10.1016/j.stem.2016.08.002 [PubMed: 27618216]

20. Kamp F, Exner N, Lutz AK, Wender N, Hegermann J, Brunner B, Nuscher B, Bartels T, Giese A, Beyer K et al. (2010) Inhibition of mitochondrial fusion by alpha-synuclein is rescued by PINK1, Parkin and DJ-1. *The EMBO journal* 29: 3571–3589 Doi 10.1038/emboj.2010.223 [PubMed: 20842103]
21. Lee VM, Trojanowski JQ (2006) Mechanisms of Parkinson's disease linked to pathological alpha-synuclein: new targets for drug discovery. *Neuron* 52: 33–38 Doi 10.1016/j.neuron.2006.09.026 [PubMed: 17015225]
22. Liu S, Sawada T, Lee S, Yu W, Silverio G, Alapatt P, Millan I, Shen A, Saxton W, Kanao T et al. (2012) Parkinson's disease-associated kinase PINK1 regulates Miro protein level and axonal transport of mitochondria. *PLoS genetics* 8: e1002537 Doi 10.1371/journal.pgen.1002537 [PubMed: 22396657]
23. Ludtmann MH, Angelova PR, Ninkina NN, Gandhi S, Buchman VL, Abramov AY (2016) Monomeric Alpha-Synuclein Exerts a Physiological Role on Brain ATP Synthase. *The Journal of neuroscience: the official journal of the Society for Neuroscience* 36: 10510–10521 Doi 10.1523/JNEUROSCI.1659-16.2016 [PubMed: 27733604]
24. Narendra D, Tanaka A, Suen DF, Youle RJ (2008) Parkin is recruited selectively to impaired mitochondria and promotes their autophagy. *The Journal of cell biology* 183: 795–803 Doi 10.1083/jcb.200809125 [PubMed: 19029340]
25. Narendra D, Walker JE, Youle R (2012) Mitochondrial quality control mediated by PINK1 and Parkin: links to parkinsonism. *Cold Spring Harbor perspectives in biology* 4: Doi 10.1101/cshperspect.a011338
26. Nguyen HN, Byers B, Cord B, Shcheglovitov A, Byrne J, Gujar P, Kee K, Schule B, Dolmetsch RE, Langston W et al. (2011) LRRK2 mutant iPSC-derived DA neurons demonstrate increased susceptibility to oxidative stress. *Cell stem cell* 8: 267–280 Doi 10.1016/j.stem.2011.01.013 [PubMed: 21362567]
27. Norris KL, Hao R, Chen LF, Lai CH, Kapur M, Shaughnessy PJ, Chou D, Yan J, Taylor JP, Engelender S et al. (2015) Convergence of Parkin, PINK1, and alpha-Synuclein on Stress-induced Mitochondrial Morphological Remodeling. *The Journal of biological chemistry* 290: 13862–13874 Doi 10.1074/jbc.M114.634063 [PubMed: 25861987]
28. Oh CK, Sultan A, Platzer J, Dolatabadi N, Soldner F, McClatchy DB, Diedrich JK, Yates JR, 3rd, Ambasudhan R, Nakamura T et al. (2017) S-Nitrosylation of PINK1 Attenuates PINK1/Parkin-Dependent Mitophagy in hiPSC-Based Parkinson's Disease Models. *Cell Rep* 21: 2171–2182 Doi 10.1016/j.celrep.2017.10.068 [PubMed: 29166608]
29. Pacelli C, Giguere N, Bourque MJ, Levesque M, Slack RS, Trudeau LE (2015) Elevated Mitochondrial Bioenergetics and Axonal Arborization Size Are Key Contributors to the Vulnerability of Dopamine Neurons. *Current biology: CB* 25: 2349–2360 Doi 10.1016/j.cub.2015.07.050 [PubMed: 26320949]
30. Paillusson S, Gomez-Suaga P, Stoica R, Little D, Gissen P, Devine MJ, Noble W, Hanger DP, Miller CCJ (2017) alpha-Synuclein binds to the ER-mitochondria tethering protein VAPB to disrupt Ca²⁺ homeostasis and mitochondrial ATP production. *Acta Neuropathol* 134: 129–149 Doi 10.1007/s00401-017-1704-z [PubMed: 28337542]
31. Polymeropoulos MH, Lavedan C, Leroy E, Ide SE, Dehejia A, Dutra A, Pike B, Root H, Rubenstein J, Boyer R et al. (1997) Mutation in the alpha-synuclein gene identified in families with Parkinson's disease. *Science* 276: 2045–2047 [PubMed: 9197268]
32. Poole AC, Thomas RE, Yu S, Vincow ES, Pallanck L (2010) The mitochondrial fusion-promoting factor mitofusin is a substrate of the PINK1/parkin pathway. *PloS one* 5: e10054 Doi 10.1371/journal.pone.0010054 [PubMed: 20383334]
33. Spillantini MG, Schmidt ML, Lee VM, Trojanowski JQ, Jakes R, Goedert M (1997) Alpha-synuclein in Lewy bodies. *Nature* 388: 839–840 Doi 10.1038/42166 [PubMed: 9278044]
34. Stowers RS, Megeath LJ, Gorska-Andrzejak J, Meinertzhagen IA, Schwarz TL (2002) Axonal transport of mitochondria to synapses depends on mltin, a novel Drosophila protein. *Neuron* 36: 1063–1077 [PubMed: 12495622]
35. Surmeier DJ, Guzman JN, Sanchez-Padilla J, Goldberg JA (2010) What causes the death of dopaminergic neurons in Parkinson's disease? *Prog Brain Res* 183: 59–77 Doi 10.1016/S0079-6123(10)83004-3 [PubMed: 20696315]

36. Surmeier DJ, Obeso JA, Halliday GM (2017) Selective neuronal vulnerability in Parkinson disease. *Nature reviews Neuroscience* 18: 101–113 Doi 10.1038/nrn.2016.178 [PubMed: 28104909]
37. Trinh K, Moore K, Wes PD, Muchowski PJ, Dey J, Andrews L, Pallanck LJ (2008) Induction of the phase II detoxification pathway suppresses neuron loss in *Drosophila* models of Parkinson's disease. *The Journal of neuroscience: the official journal of the Society for Neuroscience* 28: 465–472 Doi 10.1523/JNEUROSCI.4778-07.2008 [PubMed: 18184789]
38. Tsai PI, Course MM, Lovas JR, Hsieh CH, Babic M, Zinsmaier KE, Wang X (2014) PINK1-mediated phosphorylation of Miro inhibits synaptic growth and protects dopaminergic neurons in *Drosophila*. *Scientific reports* 4: 6962 Doi 10.1038/srep06962 [PubMed: 25376463]
39. Vives-Bauza C, Przedborski S (2011) Mitophagy: the latest problem for Parkinson's disease. *Trends in molecular medicine* 17: 158–165 Doi 10.1016/j.molmed.2010.11.002 [PubMed: 21146459]
40. Wang X, Schwarz TL (2009) Imaging axonal transport of mitochondria. *Methods in enzymology* 457: 319–333 Doi 10.1016/S0076-6879(09)05018-6 [PubMed: 19426876]
41. Wang X, Schwarz TL (2009) The mechanism of Ca²⁺-dependent regulation of kinesin-mediated mitochondrial motility. *Cell* 136: 163–174 Doi 10.1016/j.cell.2008.11.046 [PubMed: 19135897]
42. Wang X, Winter D, Ashrafi G, Schlehe J, Wong YL, Selkoe D, Rice S, Steen J, LaVoie MJ, Schwarz TL (2011) PINK1 and Parkin target Miro for phosphorylation and degradation to arrest mitochondrial motility. *Cell* 147: 893–906 Doi 10.1016/j.cell.2011.10.018 [PubMed: 22078885]

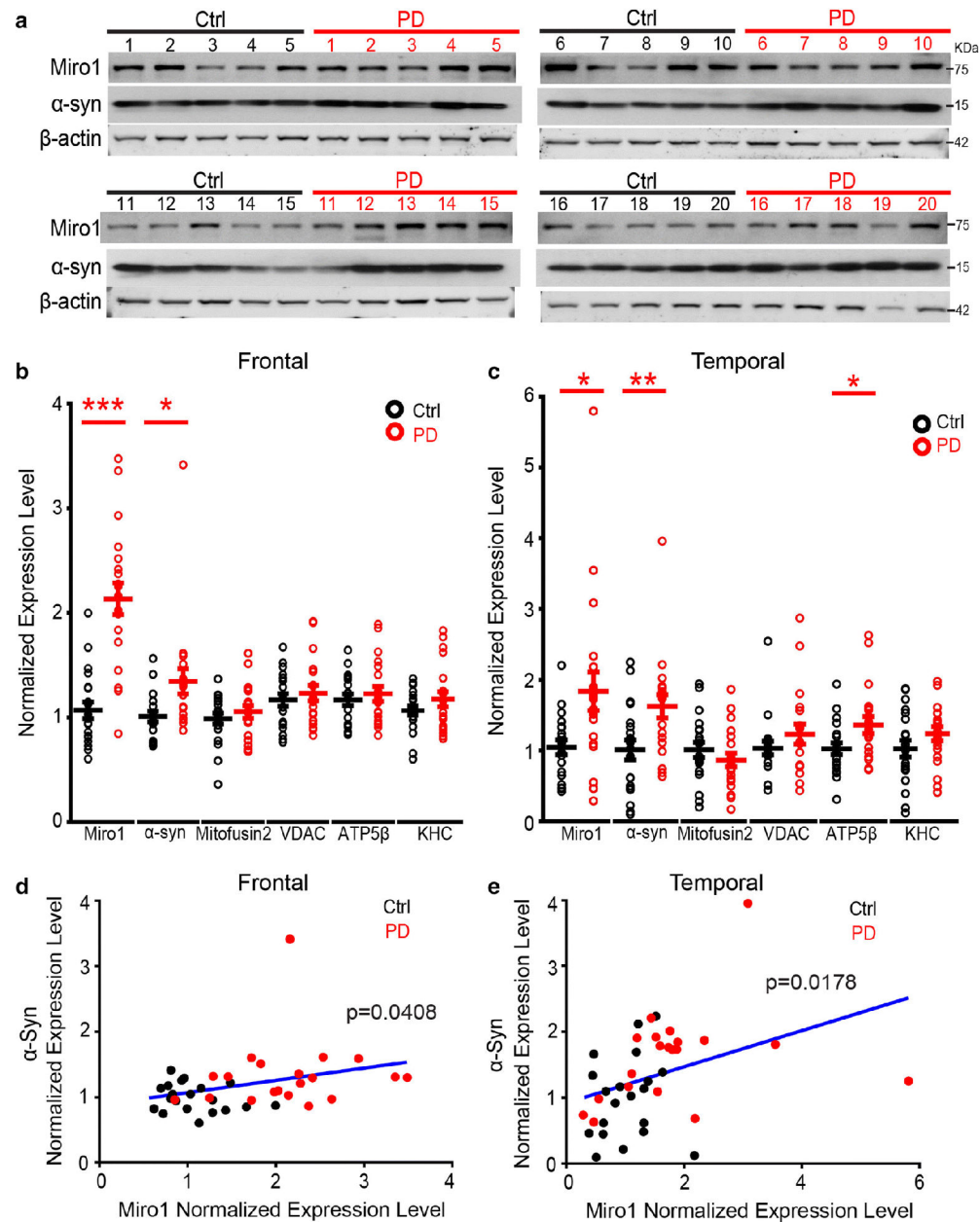
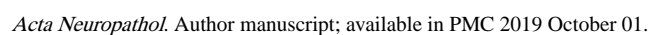
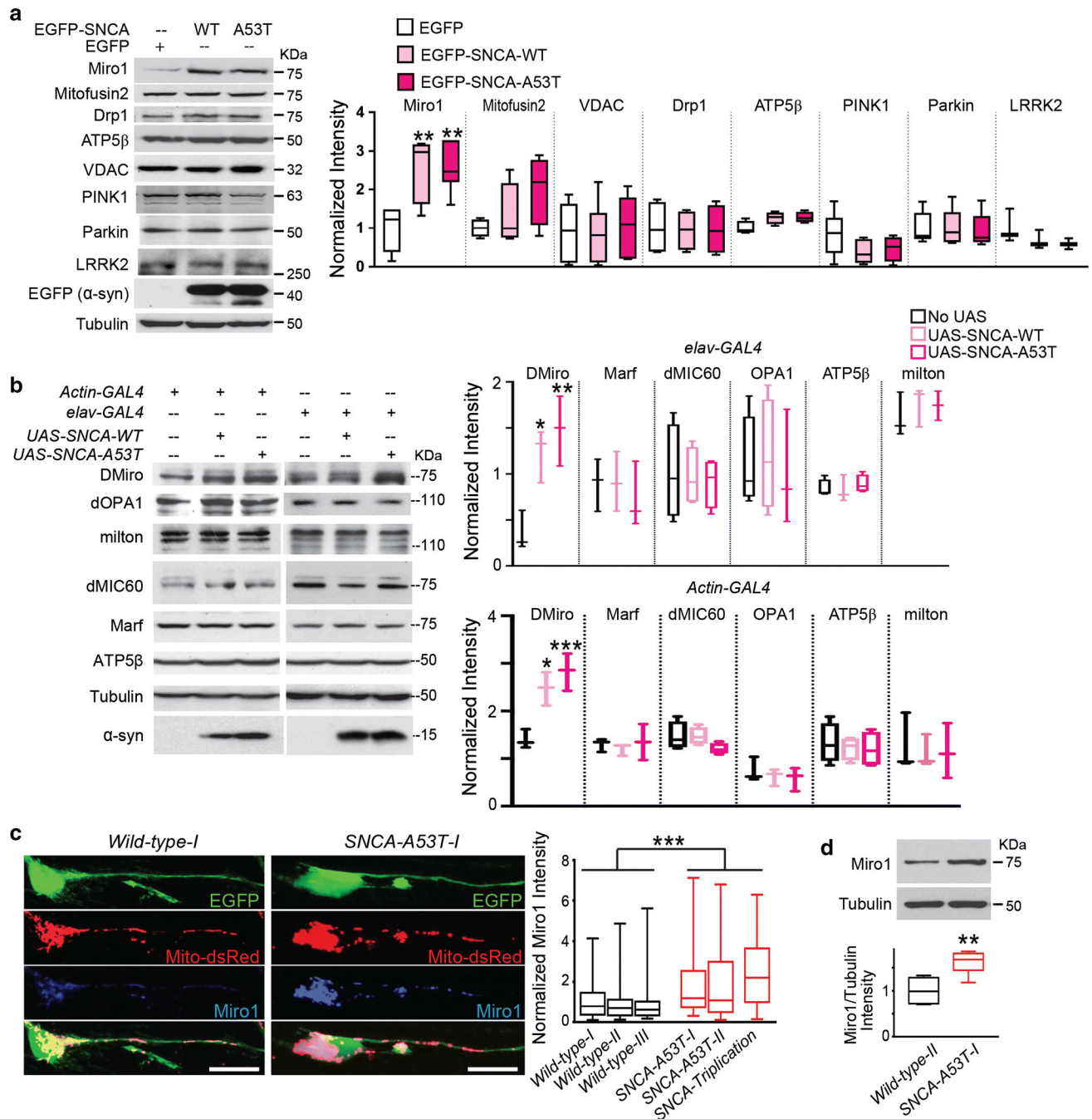


Figure 1. Miro1 Is Upregulated in Postmortem Brains of PD Patients.

(a) Frontal cortical brain lysates were analyzed by immunoblotting as indicated. (b-c) Quantification of the band intensities for the frontal cortex (b) and temporal cortex (c). Each sample was run 5–10 times in different gels, and the intensity of each band is normalized to that of actin and averaged. n=20. Mann-Whitney *U* test. The band intensities of actin are not different among all subjects ($P > 0.26$). (d, e) Correlation analysis of the Miro1 and α-syn protein levels for the frontal cortex (d) and temporal cortex (e). * $P < 0.05$, ** $P < 0.01$, *** $P < 0.001$ for all figures unless otherwise stated.





(a-b) Lysates of HEK cells (a) and of 15-day old flies (b) were immunoblotted as indicated. The band intensity of each protein is normalized to that of Tubulin from the same experiment. n=6 independent experiments for (a) and 3 for (b). For each individual experiment in (b), 12 fly heads (elav-GAL4 group) and 8 fly whole bodies (Actin-GAL4 group) were lysed. (c) iPSC-derived neurons were transfected with mito-dsRed and EGFP, immunostained with anti-Miro1, and imaged at day 22–26. The specificity of the immunostaining signals of anti-Miro1 was verified in [19] and Fig. 4b. The right panel is the

quantification of the Miro1 intensity normalized to that of mito-dsRed. The fluorescent intensities of mito-dsRed are indistinguishable among all lines ($P=0.2973$). $P<0.001$ when each mutant line is compared with every control line. $n=67-172$ neurons from 3–6 independent transfections. Scale bars: 20 μm . (d) iPSC-derived neurons 22 days after differentiation were lysed and immunoblotted. The band intensity of Miro1 was normalized to that of Tubulin from the same blot and expressed as a fraction of the mean of “*Wild-type-II*”. $n=6$. Mann-Whitney U test.

Author Manuscript

Author Manuscript

Author Manuscript

Author Manuscript

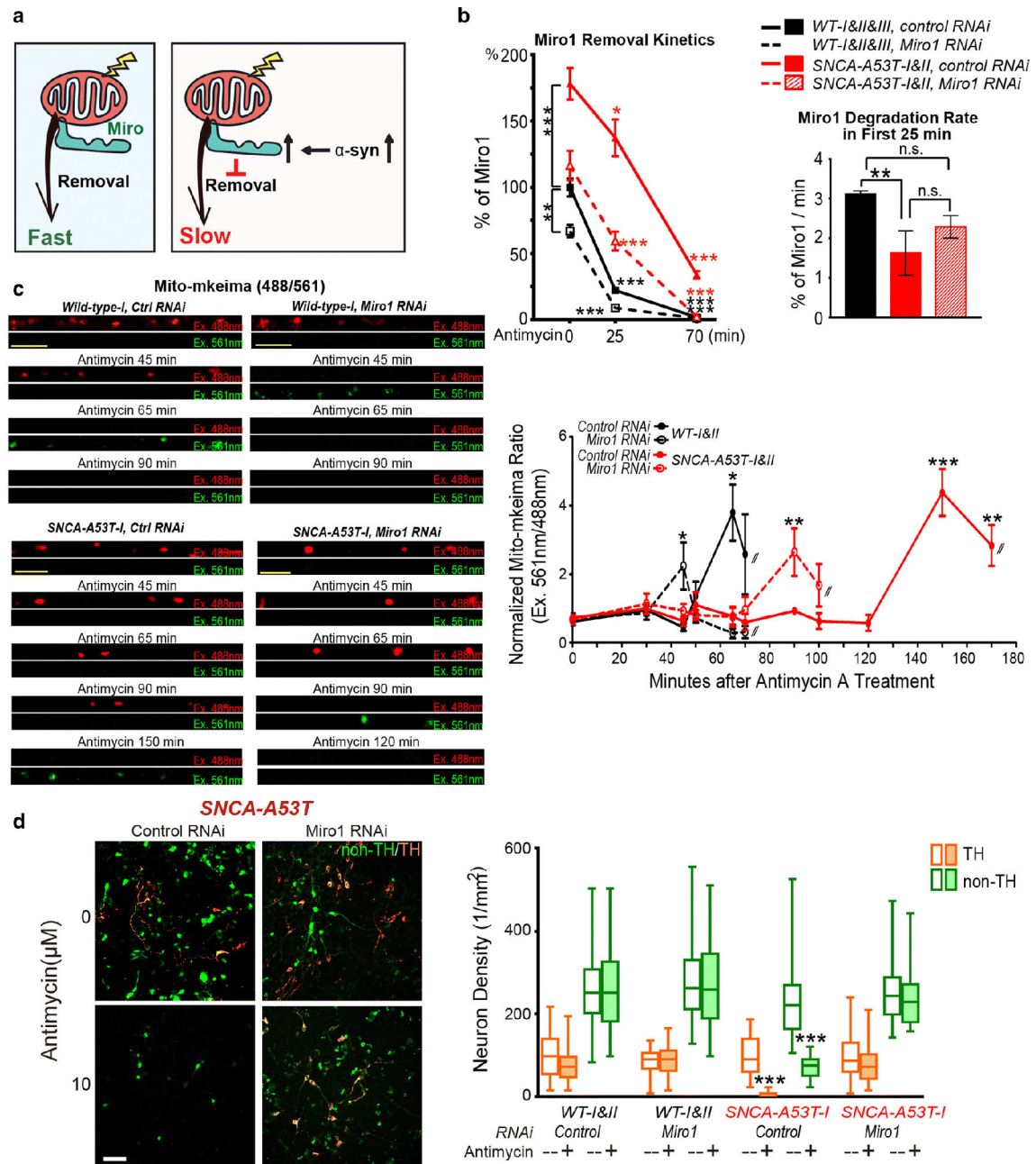
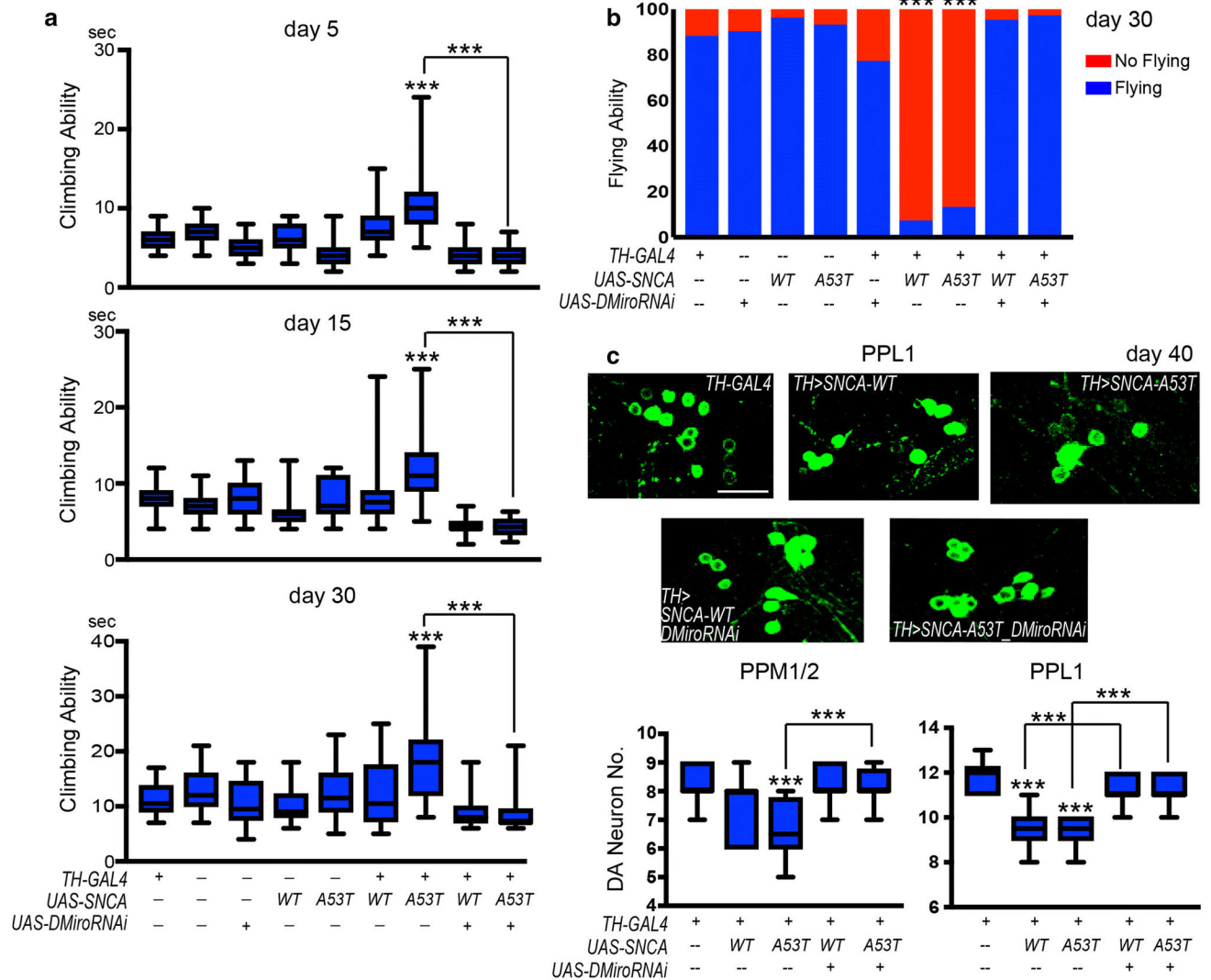


Figure 4. Miro1 RNAi Rescues Phenotypes in SNCA-A53T iPSC-Derived Neurons.

(a) Schematic representation of upregulation of Miro by α -syn expression. (b) Using immunostaining methods similar as in Fig. 3c, the Miro1 intensity normalized to that of mito-dsRed is calculated at different time points after 100 μ M Antimycin A treatment, expressed as a percentage of the mean of “WT-I&II&III, control RNAi, 0 min”. The degradation rate of Miro1 (%/min) is calculated within the first 25 min. WT: wild-type. Different lines of the same genotype are pooled. n=158–263 neurons from 6–9 independent transfections. (c) Neurons transfected with mito-mkeima are shown. The intensity ratio of mito-mkeima is measured at different time points, expressed as a fraction of the mean of “WT-I&II, control RNAi, 0 min”. Comparisons with “WT-I&II, control RNAi, 0 min”. n=6–

8 axons from 6–8 independent transfections. (d) Representative 20×magnification images of EGFP-transfected neurons, treated as indicated, and immunostained with anti-TH. The density of neurons (identified by morphology) is calculated in each condition, from 10 fields each transfection from 3–6 independent transfections. The densities of neurons without treatment (0 μ M) were not significantly different among all conditions ($p=0.4966$). Comparisons with “*WT-I&II*, control RNAi, no treatment”. Mann-Whitney *U* test. All neurons were 23–25 days after differentiation. Scale bars: (c) 10 μ m; (d) 50 μ m.



bars, n=27–70 flies. The Chi Square Test is used as the data is categorical. (c) Confocal stack images show dopaminergic (DA) neurons in adult brains in the PPL clusters immunostained with anti-TH. Quantification of the DA neuron number in both the PPL1 (one side) and PPM1/2 clusters. n=12–19 brains. One-Way ANOVA Post-Hoc Tukey test. Scale bar: 27.5 μ m. Comparisons with “*TH-GAL4*” except otherwise indicated.

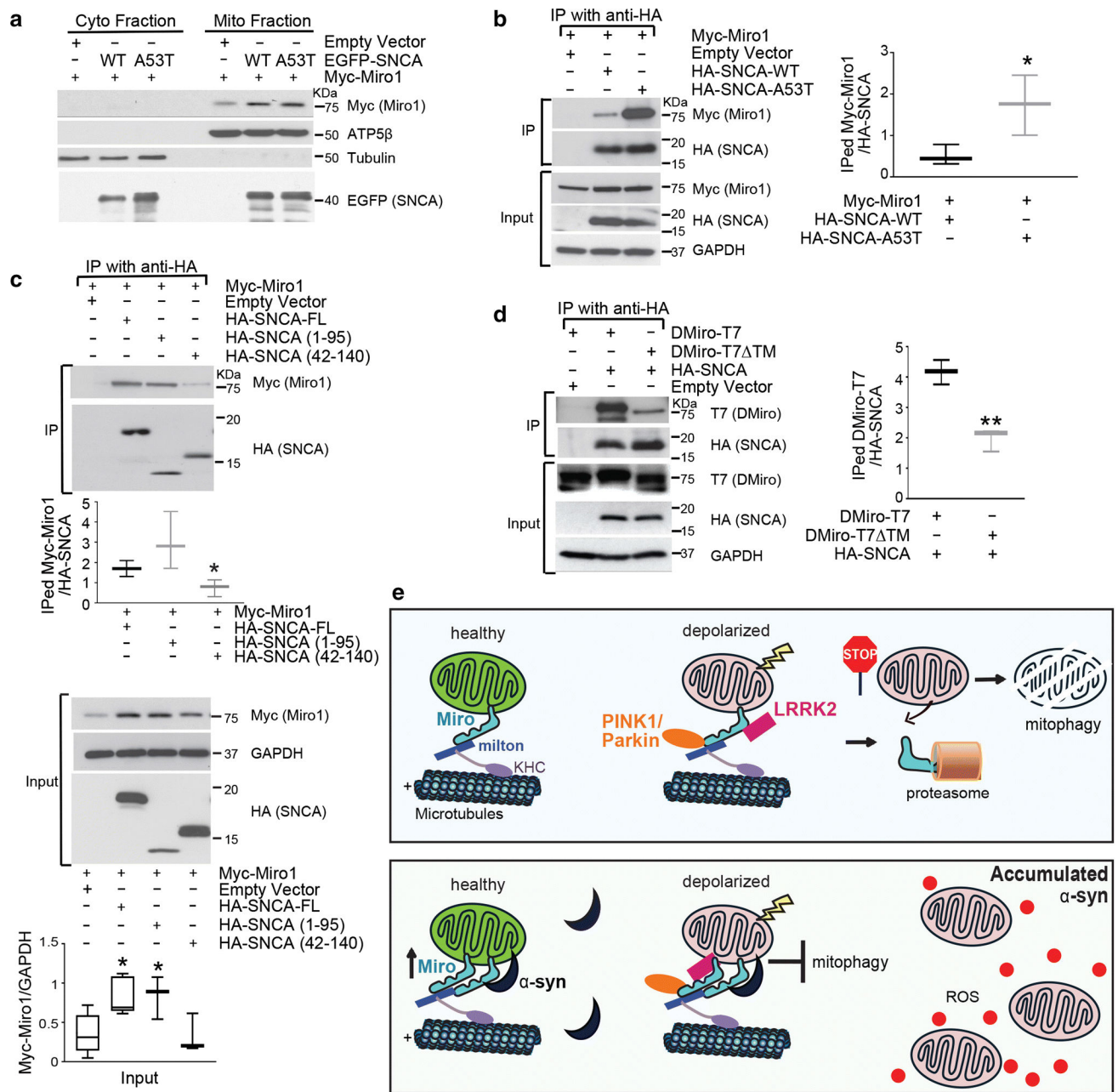


Figure 6. Miro Interacts with α -Syn.

(a) Mitochondrial fractionation shows overexpressed α -syn in the mitochondrial and cytosolic fractions. Similar results were repeated for 4 times. (b-d) HEK cells were transfected as indicated and immunoprecipitated (IP) for detecting interactions between Miro and mutant α -syn (b) or truncated α -syn (c), or between truncated DMiro and full-length α -syn (d). The band intensity of IP-ed Miro is normalized to that of IP-ed HA-SNCA. For (c), the band intensities of Myc-Miro1 in "Input" are normalized to those of GAPDH. Compared with the genotype in the far left. $n=5$ independent experiments. Mann-Whitney U test. For all experiments, an empty pcDNA3.1 vector was transfected when the SNCA vector

was not transfected. (e) Schematic representation of accumulated Miro and delayed mitophagy.

Author Manuscript

Author Manuscript

Author Manuscript

Author Manuscript